ESI

Supporting Information

Oxygen Vacancy Injection-Induced Resistive Switching in Combined Mobile and Static Gradient Doped Tin Oxide Nanorods

Thomas Herzog,[a,b] *Naomi Weitzel,*[b] *Sebastian Polarz*[*a,b]

[a.] *Leibniz-University Hannover, Institute of Inorganic Chemistry, Callinstrasse 9, 30167 Hannover, Germany, E-mail: sebastian.polarz@aca.uni-hannover.de*
[b.] *University of Konstanz, Department of Chemistry, Universitätsstrasse 10, 78457 Konstanz, Germany*

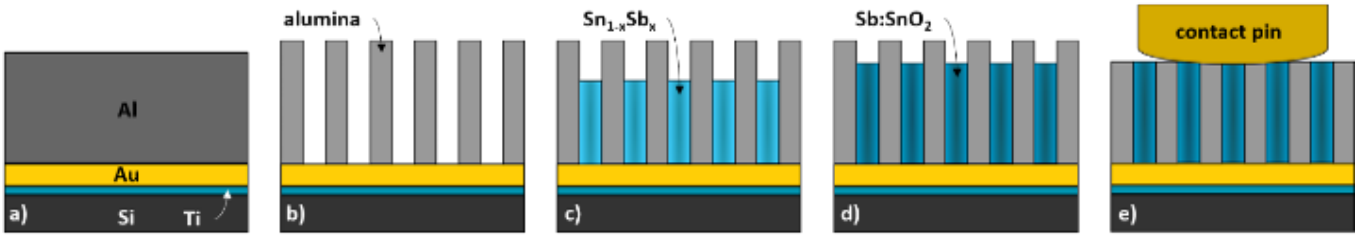

Fig. S1: Scheme of the fabrication and characterization of the microdevice consisting of porous-anodic-alumina-inbuilt antimony-doped tin oxide nanowires. a) sputter deposition of an Al/Au/Ti stacked-layer onto a Si wafer, b) formation of the porous alumina template by a two-step anodization process, c) electrodeposition of a tin-antimony alloy into the porous template, d) thermal oxidation of the alloy to obtain antimony-doped tin oxide nanowires, and e) polishing of the alumina template for exposing nanorod tips and contacting with a contact pin.

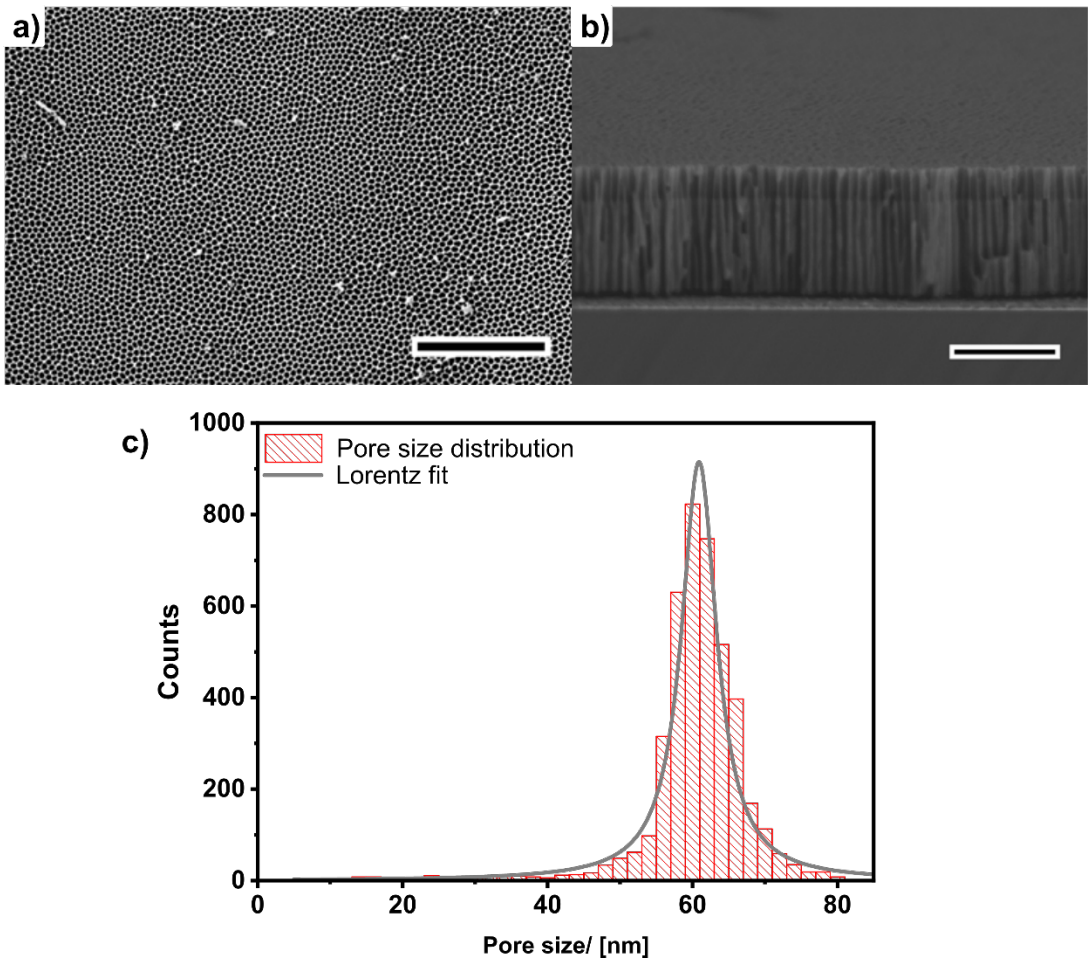

Fig. S2: Characterization of the substrate-supported AAO membrane. a) Top-view (scalebar 2 µm) and b) side-view (scalebar 1 µm) of the AAO membrane. c) Pore size distribution of the membrane with calculated Lorentz fit (maximum = 60.9 nm, Γ = 2.96)

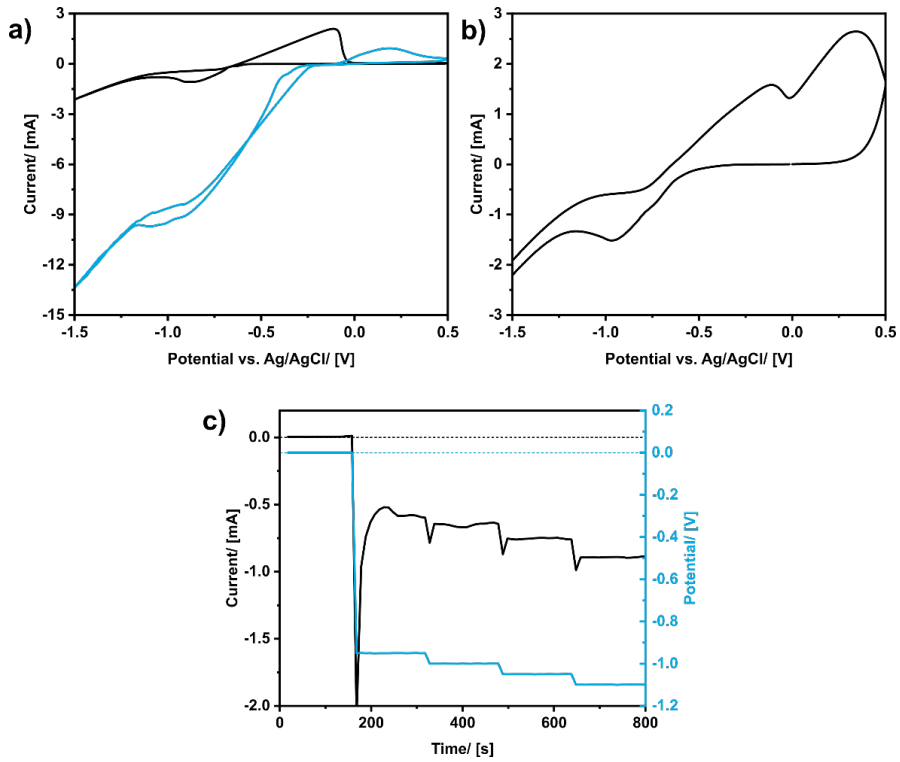

Fig. S3: Determination of the deposition conditions and deposition program. a) CV of an aqueous solution containing 0.07 M sodium citrate, 0.1 M citric acid and 0.015 M $Sb_2(SO_4)_3$ (blue) or 0.015 M $SnSO_4$ (black). b) Aqueous solution containing both metal salts (overall metal ion concentration 0.015 M). c) Deposition program and measured current profile for the formation of graded nanorods. As a working electrode, the substrate-supported AAO membrane is utilized in combination with a platinum wire as counter electrode.

The single metal ion solutions exhibit a cathodic at -0.95 V and at -0.9 V for the reduction of antimony and tin, respectively. The strong increase in current at more negative potentials can be assigned to hydrogen reduction at the working electrode. The anodic peaks can be assigned to the re-oxidation of the respective metal ions. The mixed solution exhibits only one cathodic peak, which is consistent with alloy formation. The two anodic peaks can be assigned to the re-oxidation of the metals.

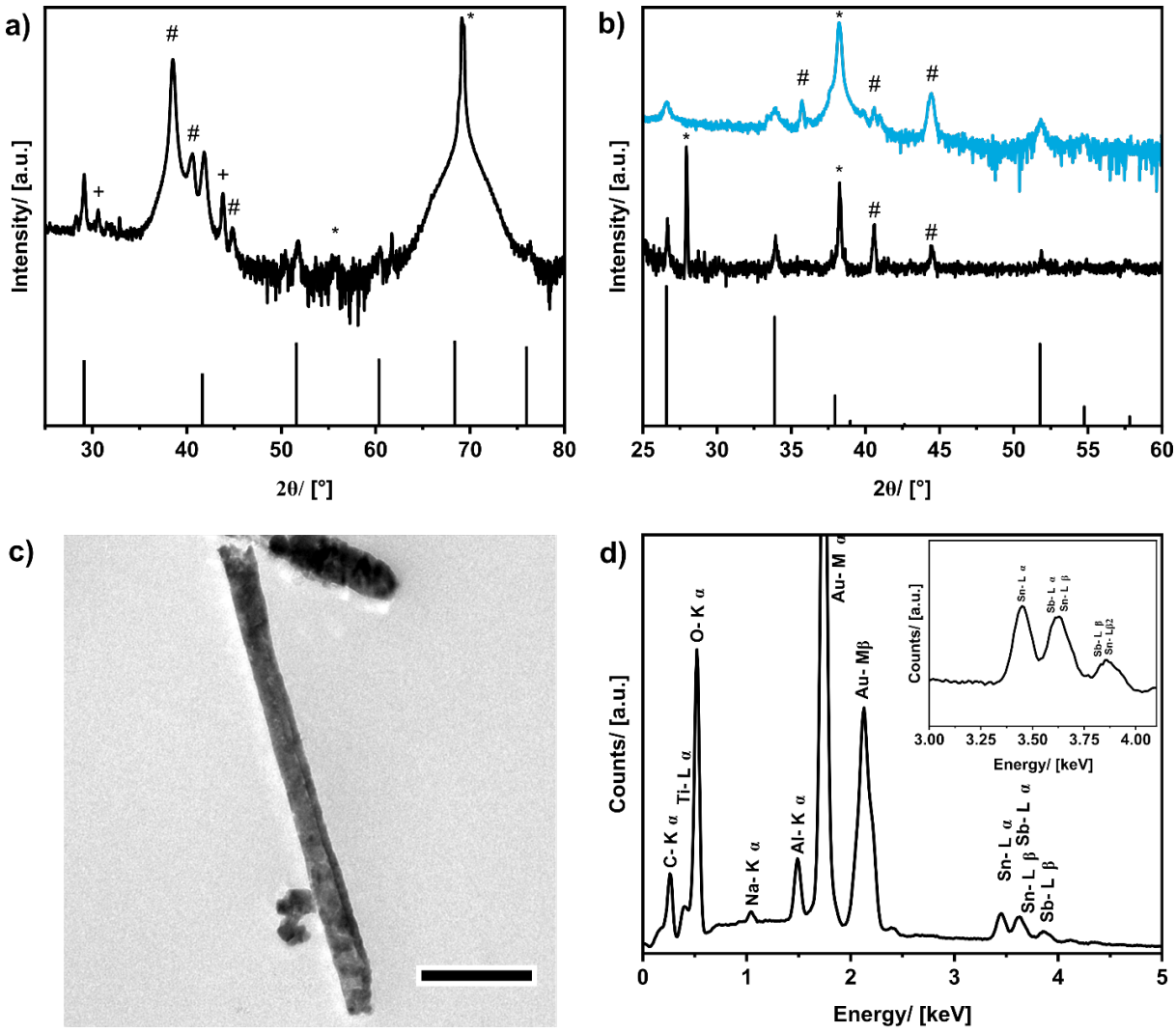

Fig. S4. Further characterization of the nanorod arrays. a) PXRD of the nanorod array before oxidation (reference: SnSb COD 9008724, * = substrate (Si/SiO2); # = coating of the substrate (Ti/Au); + = residual Sn/Sb). b) PXRD of the arrays after oxidation of the mono-domain (black) and two-domain (blue) nanorods (reference: SnO_2 casserite COD100006, * = substrate (Si/SiO2); # = coating of the substrate (Ti/Au)). c) TEM image of the oxidized mono-domain nanorods (scalebar 200 nm). d) EDX spectrum of the oxidized nanorods prepared at a deposition potential of -0.95 V (inset: magnified energy range of the Sn and Sb peaks).

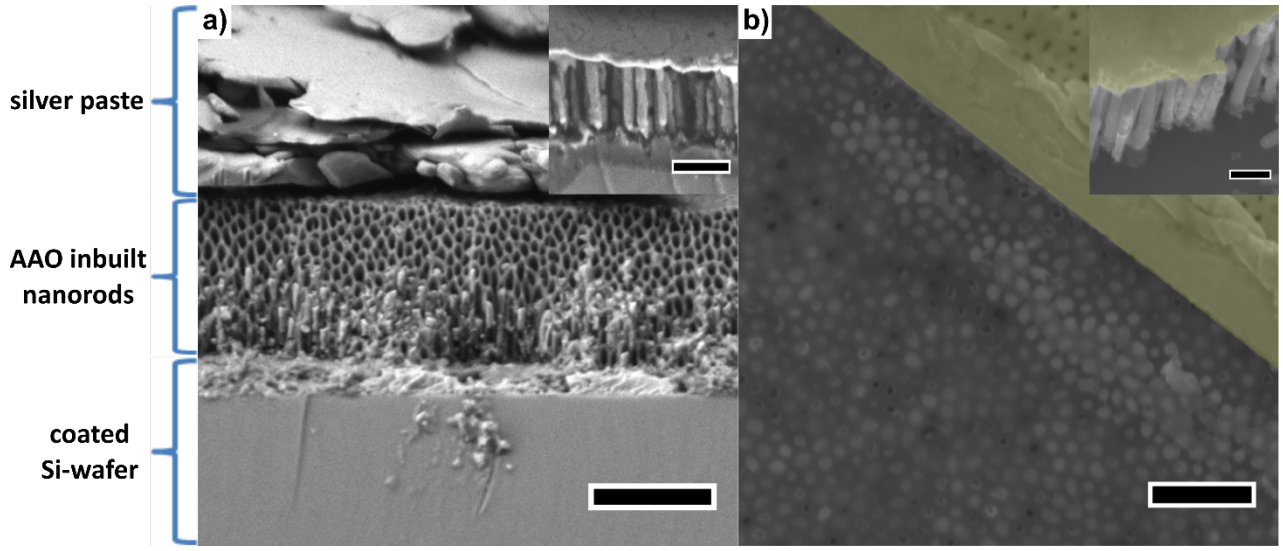

Fig. S5. SEM image of a typical nanorod device. a) Side view of a device contacted with silver conductive paste (scalebar 1 µm). Inset: Side view of the silver paste contacted device after 50 cycles of switching and removal of the AAO template (scalebar 1 µm). b) Top view of the device showing the polished surface of the template with exposed nanorod tips and the gold top contact layer (colored in yellow, scalebar 500 nm). Inset: Side view of the gold contacted device after 50 cycles of switching and removal of the AAO template (scalebar 200 nm).

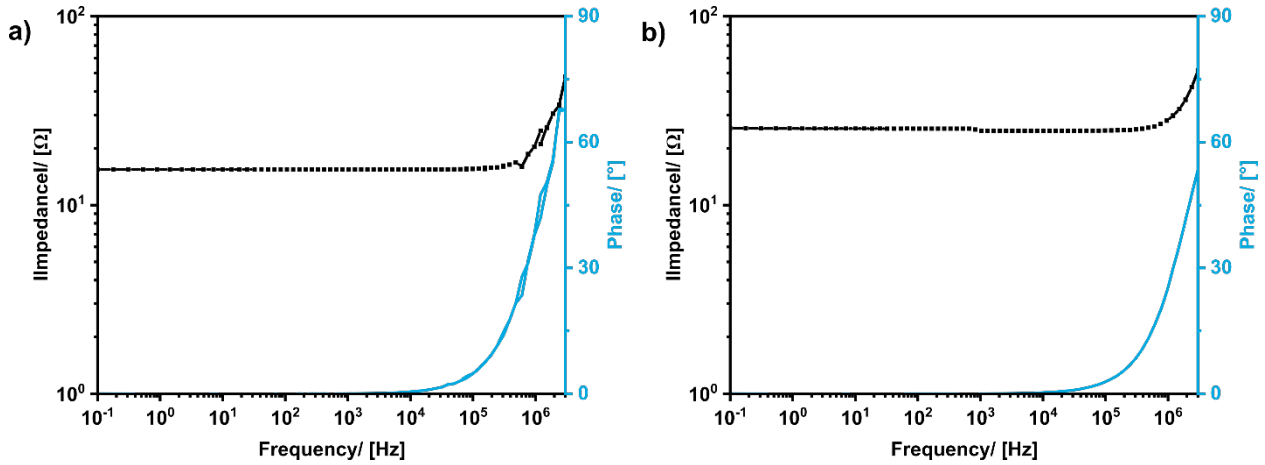

Fig. S6. Further electrical characterization of homogeneous, mono-domain ATO and graded two-domain ATO-TO nanorods. a) Impedance spectrum of the mono-domain ATO nanorods in BODE representation. Showing a small impedance of about R = 15 Ω in the low frequency regime, indicating quasi-metallic conductivity of the ATO nanorods. Inductive reactance in the high frequency regime, results in an increasing impedance for high frequencies. b) Impedance spectrum of the graded ATO nanorods in BODE representation. Showing a small impedance of about R = 25 Ω in the low frequency regime, indicating quasi-metallic conductivity of the graded ATO nanorods. Inductive reactance in the high frequency regime, results in an increasing impedance for high frequencies.

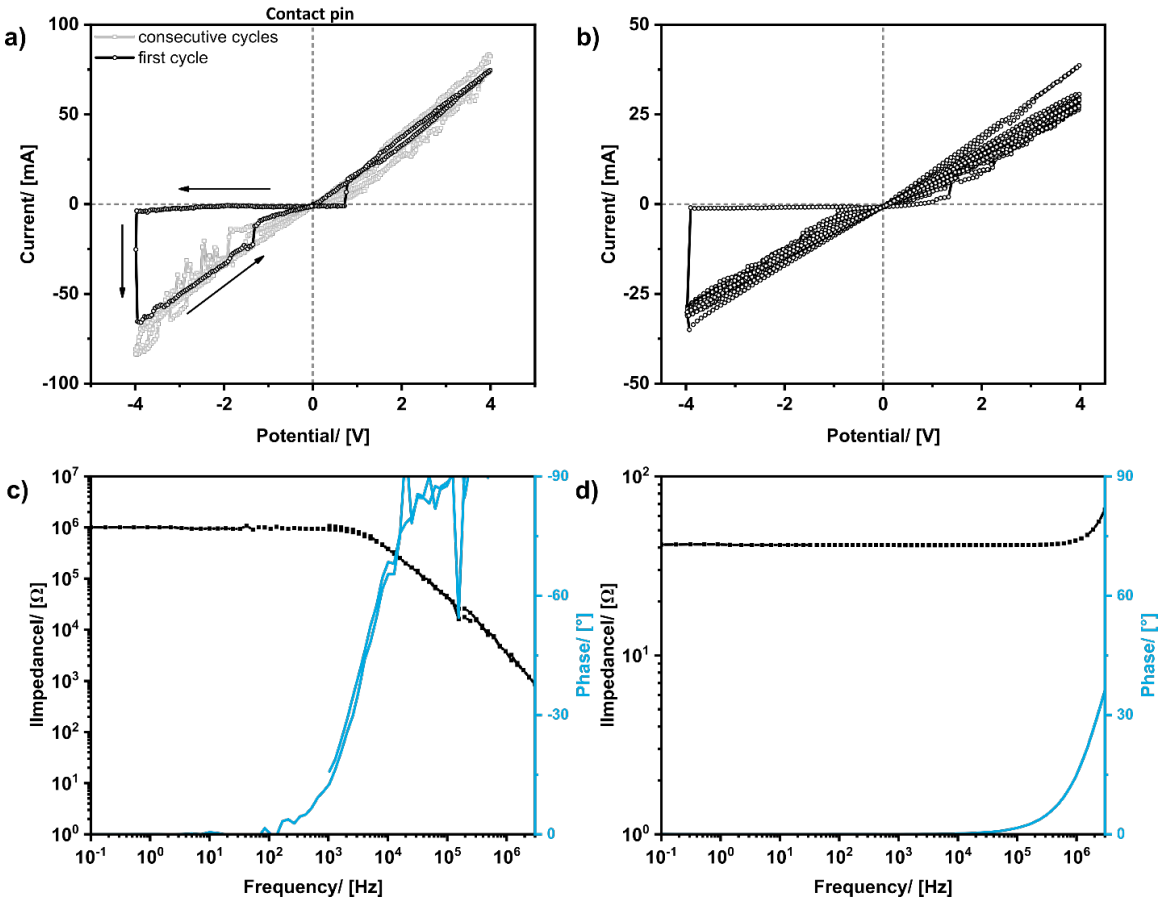

Fig. S7. Further electrical characterization of the two-domain ATO-TO nanorods with sharp junction. a) IV characteristic of the two-domain nanorods device with a sharp junction without additional silver paste layer. b) IV characteristic of the same device after thermal reset. c) Impedance spectrum of the device before switching (HRS) in BODE representation (R = 1 MΩ in the low frequency regime, the decrease in the high frequency regime is attributed to capacitive reactance. The junction and the resulting SCR can be described by an RC element, whereby the capacity element results in a decreasing impedance at increasing frequencies.) d) Impedance spectrum of the device after switching (LRS) in BODE representation (R = 40 Ω in the low frequency regime, inductive reactance in the high frequency regime, results in an increasing impedance for high frequencies.)

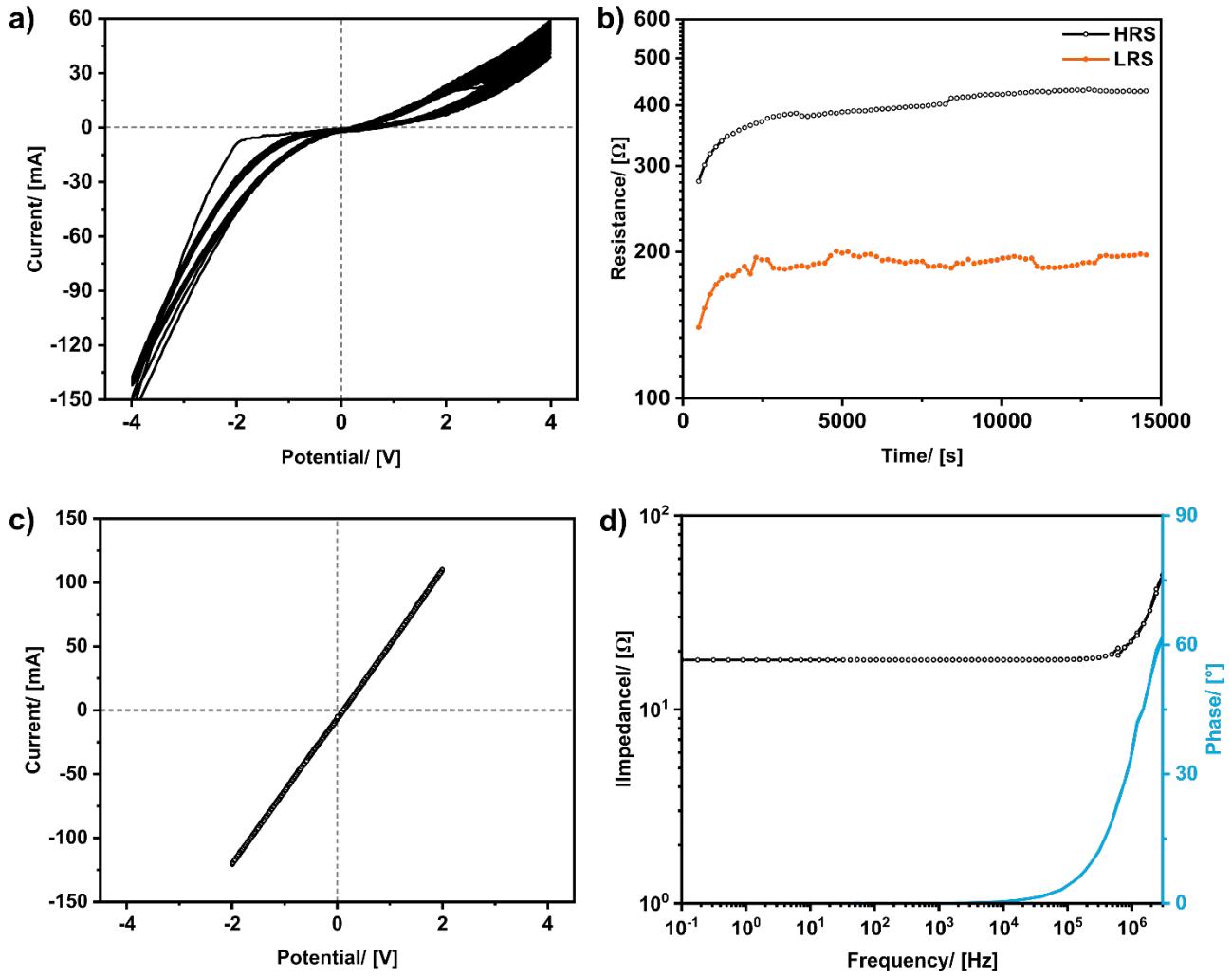

Fig. S8. Further electrical characterization of the three-segmented devices with Ag paste. a) IV characteristic of the device with the sharp junctions for 50 consecutive cycles. b) Retention characteristic of the same device. c) IV characteristic of the three-domain nanorods device with graded junctions, exhibiting Ohmic conductivity. d) Impedance spectra of this device in BODE representation (R = 18 Ω in the low frequency regime, inductive reactance in the high frequency regime, results in an increasing impedance for high frequencies).

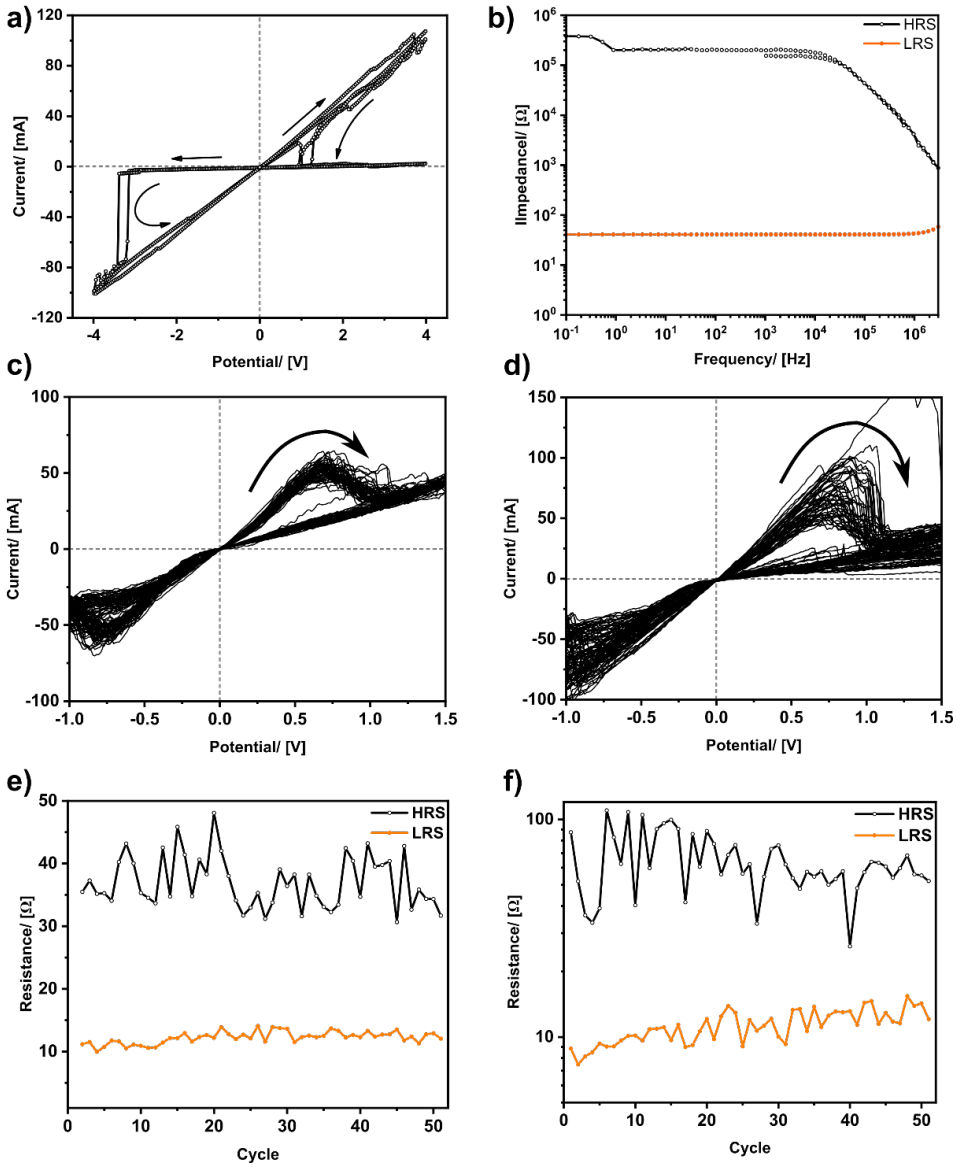

Fig. S9. Characterization of devices with alternative contacting. a) IV characteristic of the three-domain nanorods device with sharp junctions without additional silver paste layer, showing bipolar memristive switching. b) Impedance spectra of this device in HRS and LRS. c) IV characteristic of a device with a gold contact layer instead of silver paste layer (contact area 1.6 mm^2). d) IV characteristic of a device with a larger gold contact layer (contact area 5.2 mm^2). e) and f) Evolution of the resistance over 50 cycles for the devices with gold contact layer (contact area 1.6 and 5.2 mm^2, respectively).